

Grain Size and Piezoelectric Properties of (Ba, K, Na)NbO<sub>3</sub> Lead-Free Ceramics

Shinjiro TASHIRO and Keisuke ISHII

Department of Materials Science and Engineering, The National Defense Academy, 1-10-20, Hashirimizu, Yokosuka-shi 239-8686

(Ba, K, Na)NbO<sub>3</sub> 非鉛セラミックスの結晶粒径と圧電特性

田代新二郎・石井啓介

防衛大学校機能材料工学科, 239-8686 神奈川県横須賀市走水 1-10-20

Grain size and piezoelectric properties were investigated in (K, Na)NbO<sub>3</sub> ceramics substituted with Ba for K and Na by 1 to 5 mol%, in anticipation of high piezoelectric properties. The grain size strongly depended on the A/B ratio in perovskite structure. The grain growth phenomenon was markedly similar to that of BaTiO<sub>3</sub> semiconducting ceramics with donor additives. Piezoelectric properties were strongly affected by grain size. MnO additive was added to suppress grain growth anomaly, dense ceramic body formation and withstanding voltage enhancement. However, a manufacturing process, in which MnCO<sub>3</sub> was directly mixed to other raw material powders, resulted in the formation of large pores ranging to 1 mm diameter in their ceramic bodies. The powder obtained by previously calcining the mixture of Nb<sub>2</sub>O<sub>5</sub> and MnCO<sub>3</sub> was used as a raw material for MnO addition, in order to prevent the formation of large pores. By adding 0.5 mol% MnO, grain growth anomaly was inhibited, and a uniform and dense ceramic body was consequently obtained without piezoelectric property degradation. [Received January 18, 2006; Accepted March 16, 2006]

**Key-words:** Lead-free, Piezoelectric ceramic, Sr substitution, A/B ratio, KNbO<sub>3</sub>, NaNbO<sub>3</sub>, MnO addition, Grain growth anomaly, Donor dopant

## 1. Introduction

Lead zirconate titanate (PZT) ceramics have been widely used for piezoelectric applications due to their high piezoelectricity. However, the development of lead free piezoelectric ceramics is expected from global environmental considerations. The current status and prospects for bismuth layer-structured ferroelectric (BLFS) and perovskite ferroelectric ceramics in lead-free piezoelectric materials were introduced by Takenaka and Nagata.<sup>1)</sup> BLSF ceramics are restricted to ceramic filter and resonator applications due to their low piezoelectricity. On the other hand, perovskite ceramics seem to be suitable for actuator and high-power applications due to their relatively high piezoelectricity. Perovskite-type lead-free piezoelectric ceramics have been mainly investigated using KNbO<sub>3</sub>-based,<sup>2)-5)</sup> (K, Na)NbO<sub>3</sub>-based<sup>6)-13)</sup> and (Bi, Na)TiO<sub>3</sub>-based<sup>14)-22)</sup> ceramics.

(Bi, Na)TiO<sub>3</sub>-based ceramics exhibit a transition from a ferroelectric phase to an antiferroelectric phase at temperatures around 200°C, and their piezoelectricity disappears above these temperatures. Furthermore, (Bi, Na)TiO<sub>3</sub>-based ceramics are disadvantageous in that their coercive field is large, making poling difficult. Their compositions, which can easily be poled, have recently been investigated, and a relatively large piezoelectricity has been obtained.<sup>22)</sup> Although there were two serious problems, poor sinterability and deliquescence, in KNbO<sub>3</sub>-based and (K, Na)NbO<sub>3</sub>-based ceramics, their problems have been overcome through the improvement of the sample preparation process.<sup>4), 5), 8)-12)</sup>

Kimura et al. found a relatively large piezoelectricity in a KNbO<sub>3</sub>-NaNbO<sub>3</sub>-LiNbO<sub>3</sub> ternary system.<sup>12)</sup> Saito et al. also found a large piezoelectricity in a (K, Na, Li)(Nb, Ta, Sb)O<sub>3</sub> system.<sup>13)</sup> On the other hand, we investigated the piezoelectric potential of (K, Na)NbO<sub>3</sub> ceramics by substituting a small amount of Pb for K and Na.<sup>23), 24)</sup> High piezoelectric properties were consequently obtained in a composition such as (Pb<sub>0.03</sub>K<sub>0.47</sub>Na<sub>0.47</sub>)NbO<sub>3</sub> with the assumption of A-site vacan-

cies. In this study, it was experimentally investigated whether high piezoelectric properties are maintained even if Ba is used as a substituting element instead of Pb. That is, it was clarified that the high piezoelectric potential is independent of the substituting element and mainly depends on the A-site vacancy and grain size.

## 2. Experimental procedure

The material compositions used in this study are (Ba<sub>x</sub>K<sub>y</sub>Na<sub>y</sub>)NbO<sub>3</sub>, where  $y=0.5-x$  corresponds to a stoichiometry having atomic vacancies of  $x$  at an A-site in a perovskite structure. Moreover, in this study, the A/B ratio, which is a  $y$  value against an  $x$  value, was changed, as in the case of Pb substitution. Hereinafter, sample compositions are abbreviated BKN (100x/100y).

Reagent-grade metal oxide or carbonate powders, BaCO<sub>3</sub>, K<sub>2</sub>CO<sub>3</sub>, Na<sub>2</sub>CO<sub>3</sub>, Nb<sub>2</sub>O<sub>5</sub> and MnCO<sub>3</sub>, were used as starting raw materials. Since K<sub>2</sub>CO<sub>3</sub> and Na<sub>2</sub>CO<sub>3</sub> have extremely coarse particles in contrast to the fine particles of other raw materials, it is necessary to grind such powders to a particle size of 1 μm or less. Prior to mixing all the raw materials, these two materials were preground under the conditions mentioned below. A polyethylene container, 60 mm in diameter and 250 ml in capacity, was used for 1/4 mol blending. Zirconia balls of 3 mmφ and 10 mmφ (300 g each), ethanol (180 ml), and K<sub>2</sub>CO<sub>3</sub> and Na<sub>2</sub>CO<sub>3</sub> powders corresponding to 1/4 mol were placed in the container, and ball-milled for 12 h at a rotation rate of 300 rpm. After pregrinding, other raw materials were placed in the container and 20 ml of ethanol was added, and they were mixed by ball-milling for 12 h at a rotation rate of 170 rpm. The SEM image of the K<sub>2</sub>CO<sub>3</sub> and Na<sub>2</sub>CO<sub>3</sub> mixture obtained after pregrinding is shown in **Fig. 1**. They were ground down to a particle size of about 1 μm or less. The authors believe that pregrinding is important in obtaining dense ceramics without deliquescence.

Using the mixing process mentioned above, although dense

and uniform bodies were obtained in the samples not added with  $\text{MnCO}_3$ , the sample added with  $\text{MnCO}_3$  exhibited large pores and consequently a low density. The formation of large pores can be prevented using a solid solution powder of  $\text{MnO}$  and  $\text{Nb}_2\text{O}_5$  as a raw material during mixing. When  $\text{MnO}$  was added,  $\text{Nb}_2\text{O}_5$  and  $\text{MnCO}_3$  powders were mixed for 12 h in water with zirconia balls of 10 mm $\phi$  using the wet ball-milling technique and calcined at 1000°C for 4 h. The calcined powder was ground for 12 h with the same wet ball-milling technique and dried. In the case of  $\text{MnO}$  addition, this powder was used in the mixing of raw materials.

The raw materials mixed in ethanol were calcined at 900°C in air after drying. The calcined powders were ground for 12 h by ball-milling under the same conditions as those used for mixing. After drying, using polyvinyl alcohol as a binder, the calcined powders were pressed into disks 15 mm in diameter at 100 MPa. These powder compacts were fired for 2 h in air at 1110 to 1170°C. Gold electrodes were sputtered on the upper and lower surfaces of the samples for the measurement of electrical properties.

The crystal structure was determined from the powder X-ray diffraction (XRD) patterns of the sintered samples. Crystal grains were observed on the thermally etched surfaces of the sintered samples by secondary electron microscopy (SEM). Electric flux density-electric field ( $D$ - $E$ ) hysteresis loops were measured by applying 50 Hz ac fields to the samples in a silicon oil bath maintained at 120°C. The samples for the measurement of piezoelectric properties were poled by applying dc fields of 2 to 5 kV/mm for 5 min in a silicon oil bath maintained at 120°C. The electromechanical coupling factors of radial mode vibration were measured by a resonance-antiresonance method on the basis of IEEE standards using an impedance analyzer (HP-4192A). The piezoelectric

constant  $d_{33}$  was measured using a Berlincourt-type quasi-static meter at 110 Hz.

### 3. Results and discussion

#### 3.1 Influence of Ba substitution

**Table 1** shows the densities and crystal structures of the sintered samples with different Ba contents. The crystal structures change to pseudocubic with Ba contents above  $x=0.03$ . **Figure 2** shows the SEM images of the crystal grains of these samples. Large grains with sizes above 15  $\mu\text{m}$  and 30  $\mu\text{m}$  generated by grain growth anomaly can be observed in the SEM images of BKN (1/49) and BKN (2/48). On the other hand, the grains of BKN (3/47) are extremely fine, the size of which is less 1  $\mu\text{m}$ . The pseudocubic structure of BKN (3/47) is probably due to its fine grains. Thus, grain growth is extremely affected by the content of Ba as a donor, resulting in the grain growth anomaly as observed in semiconducting  $\text{BaTiO}_3$  ceramics with a donor dopant.

Drofenik and coworkers have systematically studied the grain growth anomaly of semiconducting  $\text{BaTiO}_3$  ceramics.<sup>25)-27)</sup> According to these researchers, the driving force for grain growth anomaly is the stored free surface energy of fine grains, which is released during anomalous grain growth. This surface energy is consumed in oxygen release and donor-dopant incorporation. The energy required for inducing grain growth anomaly is proportional to the amount of the donor dopant. When the stored free surface energy of fine grains is constant, a critical donor-dopant concentration exists for grain growth anomaly. Grain growth anomaly occurs when the donor-dopant concentration is lower than the critical one, since the energy required for grain growth anomaly can be supplied. This critical donor-dopant concentration is affected by the A/B ratio of the perovskite structure and the oxygen partial pressure during firing.

The critical donor-dopant concentration exists between  $x=0.02$  and 0.03, as shown in the SEM images in Fig. 2. Since the

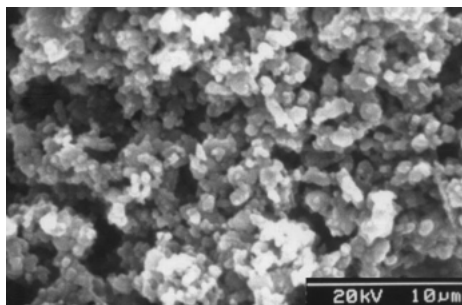


Fig. 1. SEM image of  $\text{K}_2\text{CO}_3$  and  $\text{Na}_2\text{CO}_3$  mixture ground for 12 h by ball-milling.

Table 1. Sintered Densities and Crystal Structures of Samples with Different Ba Contents

Sample	Density ( $\text{g}/\text{cm}^3$ )	Crystal structure
BKN (1 / 49)	4.37	Orthorhombic
BKN (2 / 48)	4.48	Orthorhombic
BKN (3 / 47)	4.57	Pseudocubic
BKN (5 / 45)	4.60	Pseudocubic

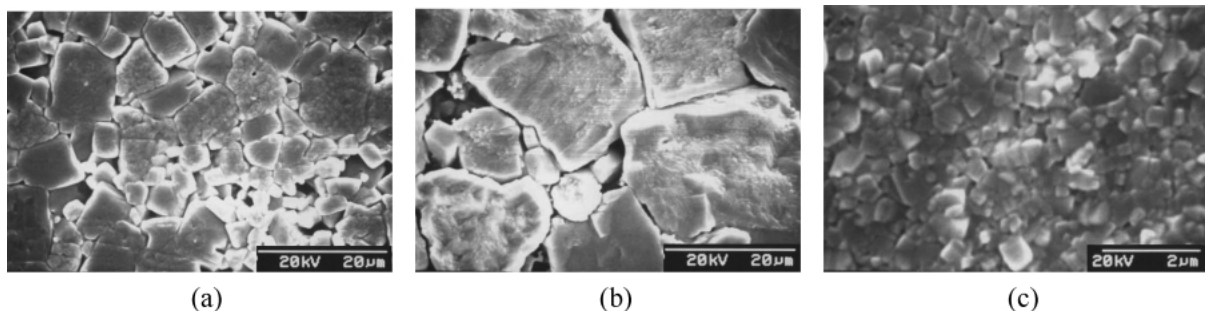


Fig. 2. SEM images of thermally etched surfaces for samples with different Ba contents. (a) BKN (1/49), (b) BKN (2/48) and (c) BKN (3/47).

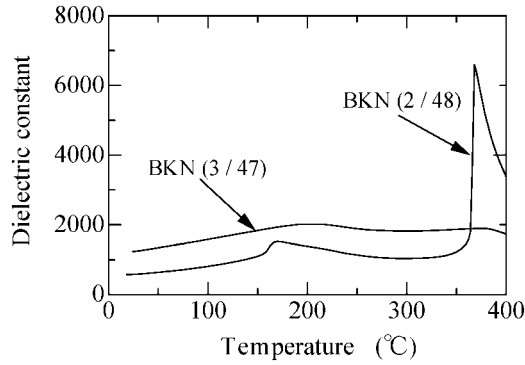


Fig. 3. Temperature dependences of dielectric constants of two samples with different in Ba contents.

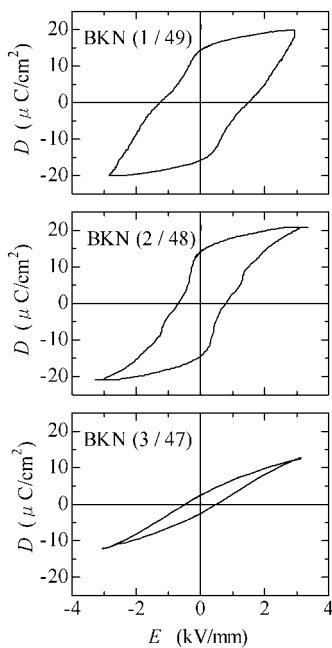


Fig. 4.  $D$ - $E$  hysteresis loops of samples with different Ba contents, measured at 50 Hz ac fields at 120°C.

critical donor-dopant concentration for grain growth anomaly is affected by the A/B ratio of the perovskite structure, it is probably possible to obtain a sample with large grains by changing the A/B ratio even though the Ba content is  $x=0.03$ .

Figure 3 shows the temperature dependences of the dielectric constants for BKN (2/48) and BKN (3/47). The dielectric constant increased up to 6600 at a Curie point for BKN (2/48). On the other hand, the temperature dependence of BKN (3/47) is broad due to its fine grains. Figure 4 shows the  $D$ - $E$  hysteresis loops at 120°C of the three samples shown in Fig. 2. Although the  $D$ - $E$  loop for BKN (1/49) seems to be not saturated from the shape, the shape is probably due to a large leak current. Shape distortion can be observed around 1 kV/mm in the applied field for BKN (2/48). This is probably caused by the mixture of fine and coarse grains as shown in Fig. 2. That is, the distortion is due to the large coercive field in fine grains and the small coercive field in large grains. The remanent polarization of BKN (3/47) is small due to its fine grains. Thus, the temperature dependences of the dielectric constant and  $D$ - $E$  hysteresis loop are mainly affected by the

Table 2. Electromechanical Coupling Factors of Radial Mode and Mechanical Quality Factors for Samples with Different Ba Contents

Sample	$k_p$	$Q_m$
BKN (1 / 49)	0.267	100
BKN (2 / 48)	0.431	153
BKN (3 / 47)	0.141	74
BKN (5 / 45)	0.116	87

Table 3. Sintered Densities and Crystal Structures of Samples with Different A/B Ratios with Same Ba Contents of  $x=0.02$  and  $x=0.03$

Ba content $x$	Sample	Density (g / cm <sup>3</sup> )	Crystal structure
0.02	BKN (2 / 49)	4.52	Pseudocubic
0.02	BKN (2 / 48.5)	4.54	Pseudocubic
0.02	BKN (2 / 48)	4.48	Orthorhombic
0.02	BKN (2 / 47.5)	4.55	Orthorhombic
0.02	BKN (2 / 47)	4.47	Orthorhombic
0.03	BKN (3 / 47)	4.63	Pseudocubic
0.03	BKN (3 / 46.5)	4.54	Pseudocubic
0.03	BKN (3 / 46)	4.57	Pseudocubic
0.03	BKN (3 / 45.5)	4.59	Orthorhombic
0.03	BKN (3 / 45)	4.60	Orthorhombic
0.03	BKN (3 / 44.5)	4.52	Orthorhombic

grain size. This agrees with the experimental results for the A/B ratio described in the next section of this paper. Table 2 shows the electromechanical coupling and mechanical quality factors. BKN (2/48) showed  $k_p=0.431$  and  $Q_m=153$ .

### 3.2 Effect of A/B ratio

As described in Section 3.1, BKN (2/48) and BKN (3/47) show extremely different grain sizes. This difference in grain size severely affects piezoelectric properties. Since the grain size is expected to change with the A/B ratio as mentioned in Section 3.1, the effect of the A/B ratio was investigated in the Ba contents of  $x=0.02$  and  $x=0.03$ . The densities and crystal structures of the sintered samples with different A/B ratios are shown in Table 3. Even with the same Ba content, the samples exhibited both pseudocubic and orthorhombic crystal structures due to the change in A/B ratio.

Figure 5 shows the SEM images of the crystal grains of the samples with different A/B ratios. The Ba content is  $x=0.02$  for samples (a), (b) and (c), and  $x=0.03$  for samples (d), (e) and (f). The grain sizes of samples (a), (d) and (e) are less than 1  $\mu\text{m}$ . These samples exhibit a pseudocubic crystal structure, as shown in Table 3. On the other hand, samples (b), (c) and (f) with large grains exhibit an orthorhombic crystal structure, as shown in Table 3. Thus, grain growth proceeds as the A/B ratio decreases, and the original crystal structure is orthorhombic.

Figure 6 shows the temperature dependences of the dielectric constants of the samples shown in Fig. 5. The temperature dependences of BKN (2/49), BKN (3/46) and BKN (3/47) are broad due to their fine grains. On the other hand, BKN (2/48), BKN (2/47) and BKN (3/45) with large grains show sharp peaks at around Curie points. The  $D$ - $E$  hysteresis loops

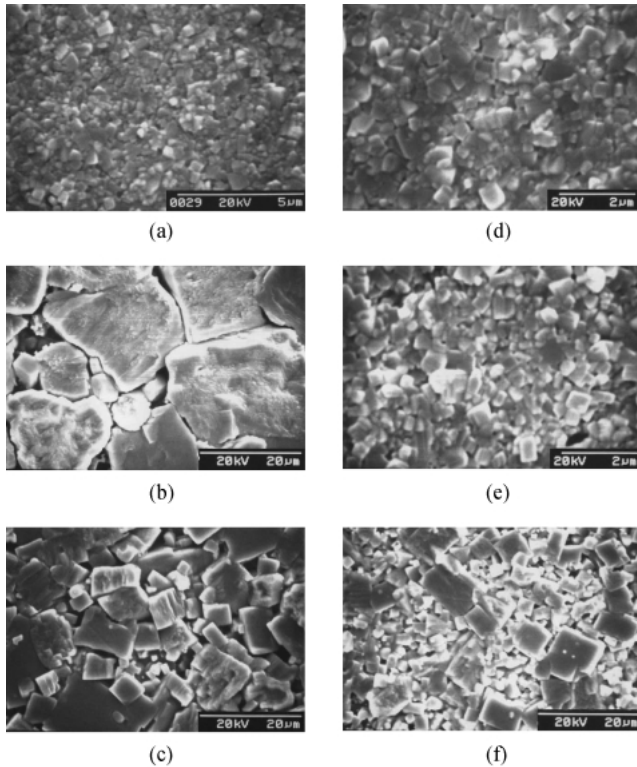


Fig. 5. SEM images of thermally etched surfaces of samples with different A/B ratios and same Ba contents of  $x=0.02$  and  $x=0.03$ . (a) BKN (2/49), (b) BKN (2/48) and (c) BKN (2/47) with Ba content of  $x=0.02$ . (d) BKN (3/47), (e) BKN (3/46) and (f) BKN (3/45) with Ba content of  $x=0.03$ .

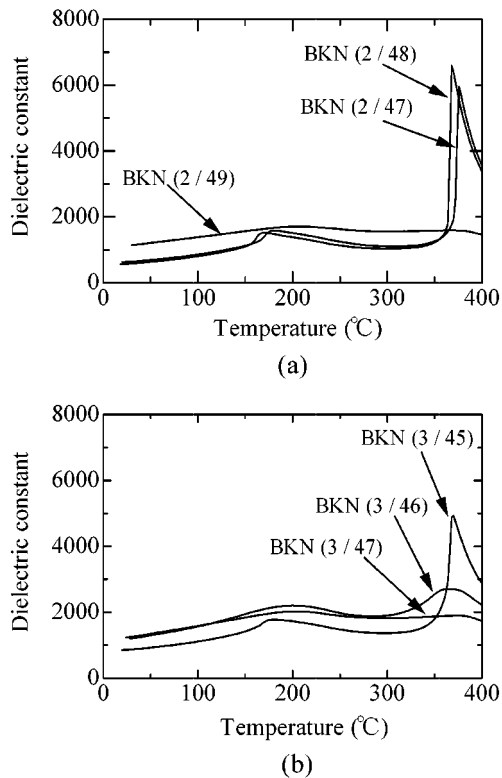


Fig. 6. Temperature dependences of dielectric constants of samples with different A/B ratios and same Ba contents of  $x=0.02$  (a) and  $x=0.03$  (b).

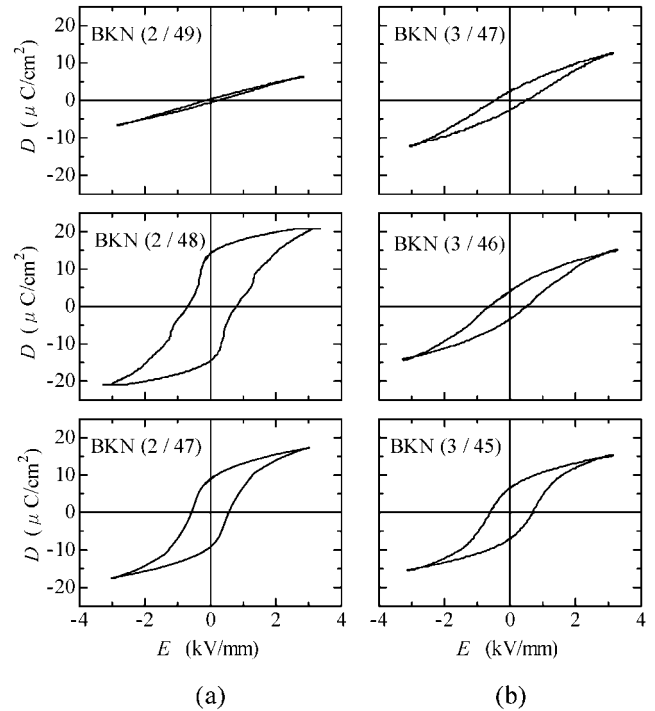


Fig. 7.  $D$ - $E$  hysteresis loops of samples with different A/B ratios with same Ba contents of  $x=0.02$  (a) and  $x=0.03$  (b).

at  $120^{\circ}\text{C}$  of the same samples are shown in Fig. 7. Remanent polarization increases with grain size and the peak value of the dielectric constant at a Curie point in Fig. 6.

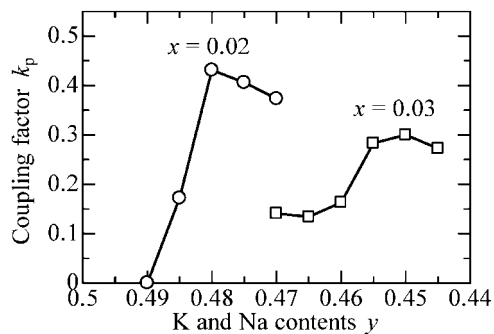
Figures 8 and 9 show the changes in piezoelectric properties with the decrease in A/B ratio. The horizontal scale is expressed with K and Na contents,  $y$ , instead of the A/B ratio. Maximum  $k_p$  and  $d_{33}$  values exist at a K and Na content. The decrease in piezoelectric properties in the left-hand side region, in which  $y$  is greater than the K and Na contents showing maximum  $k_p$  and  $d_{33}$  values, is due to the fine grain size. The decrease in piezoelectric properties in the right-hand side region, in which  $y$  is less than the K and Na contents, is considered to be induced by a second phase formed due to the lack of A-site atoms. From these experimental results in Sections 3.1 and 3.2, the optimum Ba content was determined to be  $x=0.02$  for a large piezoelectricity.

### 3.3 Influence of MnO additive

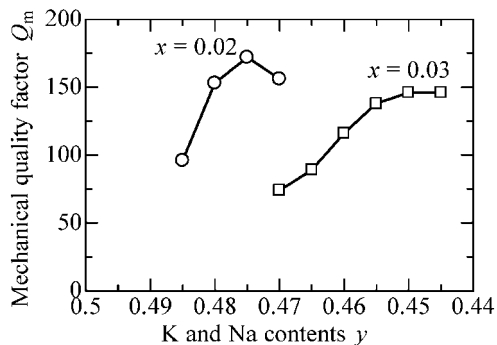
BKN (2/48) showed the largest piezoelectricity, as shown in Figs. 8 and 9. However, BKN (2/48) showed a mixture of large grains with sizes exceeding  $30\ \mu\text{m}$  and fine grains with sizes from 1 to  $2\ \mu\text{m}$ , as shown in Fig. 2. The ceramic containing such large and fine grains also exhibited large pores and became mechanically weak. It is desired that a ceramic body is dense and has uniform grains for high-reliability piezoelectric materials. Hence, 0.5 mol% MnO was added to BKN (2/48).

The density of the sample fired at  $1160^{\circ}\text{C}$  for 2 h was  $\rho=4.59\ \text{g}/\text{cm}^3$ . This density is higher by 2.5% than that of BKN (2/48) without MnO. Figure 10 shows the SEM image of crystal grains. Grain sizes range from 3 to  $7\ \mu\text{m}$ , and grain growth anomaly cannot be observed. Thus, the microstructure was improved by MnO addition.

The resistivity at  $120^{\circ}\text{C}$ , which calculated from the applied voltage and current during poling, was increased from  $4\sim 6\times 10^8$  to  $5\sim 7\times 10^9\ \Omega\text{cm}$  by adding 0.5 mol% MnO. The with-standing voltage also increased, which allowed us to apply an



(a)



(b)

Fig. 8. Coupling and mechanical quality factors of samples with same Ba contents of  $x=0.02$  and  $x=0.03$  as functions of K and Na contents.

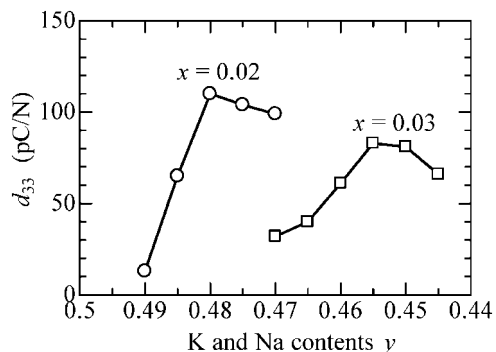


Fig. 9. Piezoelectric  $d_{33}$  constants of samples with same Ba contents of  $x=0.02$  and  $x=0.03$  as functions of K and Na contents.

electric field of 5 kV/mm at 120°C during poling. These improvements in insulation properties were achieved using Mn ions as an acceptor. That is,  $Mn^{2+}$  or  $Mn^{3+}$  ions probably compensated the electrons released from donor impurities or ionized oxygen vacancies.

Figure 11 shows the  $D-E$  hysteresis loop. The distortion in the  $D-E$  loop disappeared, although it was observed in the BKN (2/48) without MnO. This is probably due to the uniform grain size. The remanent polarization and coercive field were increased up to  $19 \mu C/cm^2$  and 1.0 kV/mm by adding 0.5 mol% MnO, respectively. The increase in coercive field is probably induced by the pinning effect of domain walls due to the increase in the number of oxygen vacancies generated by MnO addition.

Figure 12 shows the resonance-antiresonance characteristics

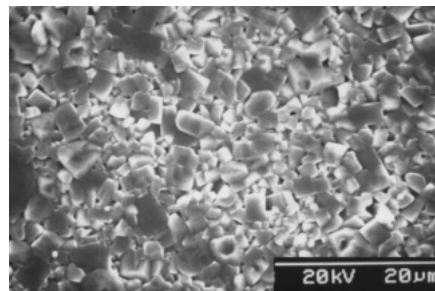


Fig. 10. SEM image of thermally etched surface of BKN (2/48) with 0.5 mol% MnO fired at 1160°C for 2 h.

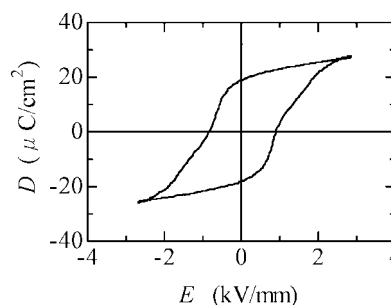


Fig. 11.  $D-E$  hysteresis loop of BKN (2/48) with 0.5 mol% MnO fired at 1160°C for 2 h.

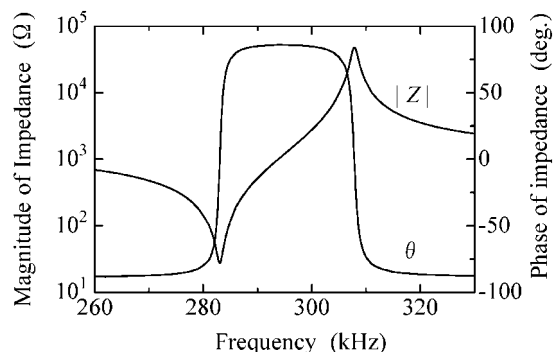


Fig. 12. Resonance-antiresonance characteristics for radial mode vibration of BKN (2/48) with 0.5 mol% MnO fired at 1160°C for 2 h. The sample was poled at 5 kV/mm at 120°C for 5 min.

for radial mode vibration. The coupling and mechanical quality factors, induced by these resonance-antiresonance characteristics, were  $k_p=0.443$  and  $Q_m=255$ , respectively. The permittivity and piezoelectric constant in the poling direction were  $\epsilon_{33}^T/\epsilon_0=471$  and  $d_{33}=124$  pC/N, respectively.

#### 4. Conclusions

In the ceramics substituted with 2 or 3 mol% Ba for an A-site of BKN (2/48), grain growth was observed greatly to be affected by the A/B ratio. The samples with grain sizes less  $1 \mu m$  showed a low piezoelectricity. Thus, it is considered necessary to realize appropriate grain growth for achieving a high piezoelectricity. The addition of 0.5 mol% MnO suppressed grain growth anomaly, resulting in the formation of dense bodies with uniform grains. However, it is essential to use the solid solution powder obtained by calcining  $MnCO_3$

and Nb<sub>2</sub>O<sub>5</sub>, as a raw material for mixing. The sample substituted with 2 mol% Ba and added with 0.5 mol% MnO showed  $k_p = 0.443$ ,  $Q_m = 255$ ,  $\varepsilon_{33}^T/\varepsilon_0 = 471$  and  $d_{33} = 124$  pC/N.

#### References

- 1) Takenaka, T. and Nagata, H., *J. Eur. Ceram. Soc.*, Vol. 25, pp. 2693–2700 (2005).
- 2) Wada, S., Seike, A. and Tsurumi, T., *Jpn. J. Appl. Phys.*, Vol. 40, pp. 5690–5697 (2001).
- 3) Ishii, H., Nagata, H. and Takenaka, T., *Jpn. J. Appl. Phys.*, Vol. 40, pp. 5660–5663 (2001).
- 4) Kakimoto, K., Masuda, I. and Ohsato, H., *Jpn. J. Appl. Phys.*, Vol. 42, pp. 6102–6105 (2003).
- 5) Kakimoto, K., Masuda, I. and Ohsato, H., *J. Eur. Ceram. Soc.*, Vol. 25, pp. 2719–2722 (2005).
- 6) Egerton, L. and Dillon, D. M., *J. Am. Ceram. Soc.*, Vol. 42, pp. 438–442 (1959).
- 7) Jaeger, R. E. and Egerton, L., *J. Am. Ceram. Soc.*, Vol. 45, pp. 209–213 (1962).
- 8) Guo, Y., Kakimoto, K. and Ohsato, H., *Appl. Phys. Lett.*, Vol. 85, pp. 4121–4123 (2004).
- 9) Guo, Y., Kakimoto, K. and Ohsato, H., *Solid State Communications*, Vol. 129, pp. 279–284 (2004).
- 10) Park, S., Ahn, C., Nahm, S. and Song, J., *Jpn. J. Appl. Phys.*, Vol. 43, pp. L1072–L1074 (2004).
- 11) Wang, R., Xie, R., Sekiya, T. and Shimojo, Y., *Jpn. J. Appl. Phys.*, Vol. 41, pp. 7119–7122 (2002).
- 12) Kimura, M., Ando, A., Shiratsuyu, K. and Sakabe, Y., *Trans. Mater. Res. Soc. Jpn.*, Vol. 29, pp. 1049–1054 (2004).
- 13) Saito, Y., Takao, H., Tani, T., Nonoyama, T., Takatori, K., Homma, T., Nagaya, T. and Nakamura, M., *Nature*, Vol. 432, pp. 84–87 (2004).
- 14) Takenaka, T., Maruyama, K. and Sakata, K., *Jpn. J. Appl. Phys.*, Vol. 30, pp. 2236–2239 (1991).
- 15) Takenaka, T., Okuda, T. and Takegahara, K., *Ferroelectrics*, Vol. 196, pp. 495–498 (1997).
- 16) Nagata, H. and Takenaka, T., *Jpn. J. Appl. Phys.*, Vol. 36, pp. 6055–6057 (1997).
- 17) Nagata, H. and Takenaka, T., *Jpn. J. Appl. Phys.*, Vol. 37, pp. 5311–5314 (1998).
- 18) Sasaki, A., Chiba, T., Mamiya, Y. and Otsuki, E., *Jpn. J. Appl. Phys.*, Vol. 38, pp. 5564–5567 (1999).
- 19) Wang, X., Tang, X. G. and Chan, H. L. W., *Appl. Phys. Lett.*, Vol. 85, pp. 91–93 (2004).
- 20) Wang, X., Chan, H. L. W. and Choy, C. L., *J. Am. Ceram. Soc.*, Vol. 86, pp. 1809–1811 (2003).
- 21) Wang, X., Kwok, K. W., Tang, X. G., Chan, H. L. W. and Choy, C. L., *Solid State Communications*, Vol. 129, pp. 319–323 (2004).
- 22) Nagata, H., Yoshida, M., Makiuchi, Y. and Takenaka, T., *Jpn. J. Appl. Phys.*, Vol. 42, pp. 7401–7403 (2003).
- 23) Tashiro, S., Nagamatsu, H. and Nagata, K., *Jpn. J. Appl. Phys.*, Vol. 41, pp. 7113–7118 (2002).
- 24) Tashiro, S. and Nagata, K., *Jpn. J. Appl. Phys.*, Vol. 43, pp. 6711–6715 (2004).
- 25) Drogenik, M., *J. Am. Ceram. Soc.*, Vol. 73, pp. 1587–1592 (1990).
- 26) Drogenik, M., *J. Am. Ceram. Soc.*, Vol. 76, pp. 123–128 (1993).
- 27) Drogenik, M., Makovec, D., Zajc, I. and Langhammer, H. T., *J. Am. Ceram. Soc.*, Vol. 85, pp. 653–660 (2002).